ASPECTS OF PLASTICITY AND FRACTURE UNDER BENDING IN Al ALLOYS

D.J. Lloyd
Aluminum Materials Consultants
Bath, Ontario

(Corresponding author: almatcon@gmail.com)

ABSTRACT

Bending is involved in the forming of many sheet parts and it is important to understand the phenomena involved. In this paper the basic equations describing bending on a global scale are compared with strain measurements of bent sheet. The development of strain on a local, microstructural scale is also investigated, as is the general aspects of plasticity and the failure process. It is shown that the global equations can be used to estimate the strains involved and the local strains can be attributed to various aspects of the plasticity. The bendability can be related to the fracture strain of the sheet and the ability of a sheet alloy to accommodate the necessary bending to form the part can be assessed.

KEYWORDS

Bending, Plasticity, Fracture, 6000 series alloys.

INTRODUCTION

The ability of a sheet alloy to undergo bending without failure is an important capability in the forming of many parts and it is useful to be able to assess the bendability of an alloy during its development. The basic mechanics of bending were developed in the 1950s (Lubhan & Sachs, 1950; Hoffman & Sachs, 1953). When a sheet is bent the upper bend surface is in tension, the lower surface in compression and at some point within the sheet there is a plane of zero strain which is referred to as the neutral axis. For sheet exhibiting limited plasticity the neutral axis is static and occurs at the mid-point of the sheet thickness but for sheet exhibiting extensive plasticity the neutral axis progresses deeper in to the sheet as bending progresses. This results in two expressions for the maximum strain at the upper bend surface depending on the motion of the neutral axis. For Al alloys such as AA6111, AA6016 and the like extensive plasticity occurs and the neutral axis is expected to move during bending. However, very few studies have examined how the neutral axis motion and the strains develop, compared with the mechanics analysis. Geist and Parker (1984) used hardness measurements to investigate neutral axis motion but these experiments did not have the resolution necessary to compare the results with experiment but did indicate neutral axis motion. To understand the nature of plasticity and failure during bending it is important to know the extent of neutral axis motion, the scale of strain gradients developed through the sheet and the maximum strains occurring at the bend surface, finally comparing experimental results with the theoretical predictions. The influence of microstructure on the evolution of strain and failure can then be considered in the context of these parameters. Recently, bending in some automotive Al alloys has been reported mainly from the microstructural perspective (Lloyd, 2000, Lloyd et al., 2002, Mattei et al., 2013) and FEM studies have also investigated the development of plasticity under bending, demonstrating the tendency for strain localization (Becker, 1992, Shi et al., 2014).

In the present paper the distribution of strain has been measured at high spatial resolution using an in-situation SEM bending technique, the strains compared with theory and approaches to predict bendability are developed.

EXPERIMENT

The Al wrought alloy AA6111, nominally (Al-0.7wt%Mg-0.6wt%Si-0.2wt%Fe-0.2wt%Mn), in the T4 temper at 1mm sheet thickness was used for the experiments. The specimen surface for examination, which was either the through thickness plane for the neutral axis study or the outer surface plane for the bending strain, was metallographically polished then electropolished. The sample was then placed in a SEM and a grid of carbon contamination spots was generated on the surface to be examined by incrementally rastering the SEM beam horizontally and vertically across the sample surface. This produces a grid of carbon spots; for the through thickness section the grid was 200 μm in the major strain direction, by 25 μm in the thickness direction, while on the bend surface a square grid of 10 by 10 μm was typically generated with a 5 by 5 μm in a few cases. A typical grid is shown in Figure 1.
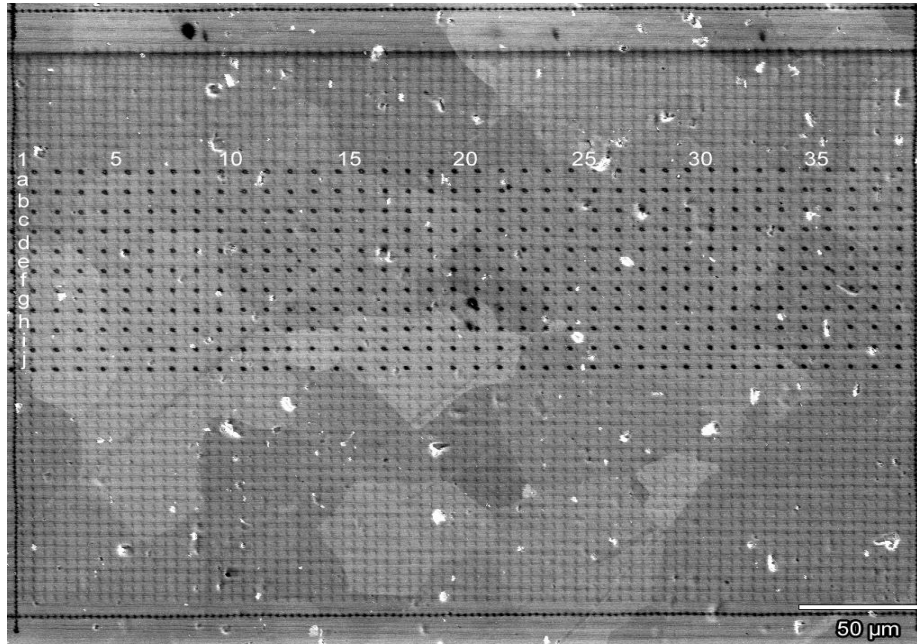
Figure 1. Carbon spot grid

Bending was carried out using a 3-Point bending apparatus, Figure 2, situated within the SEM and the progression of bending was monitored using an infrared camera viewing the bending rig through a side port of the SEM. This enabled the bending angle to be measured prior to imaging the grid for different bend angles using conventional SEM. From a digital image of the grid the position of each spot was given a pair of X,Y co-ordinates electronically and with initial and final positions of the carbon spots recorded, the level of strain was calculated. Conventional bend tests were carried out using a wrap bend test.
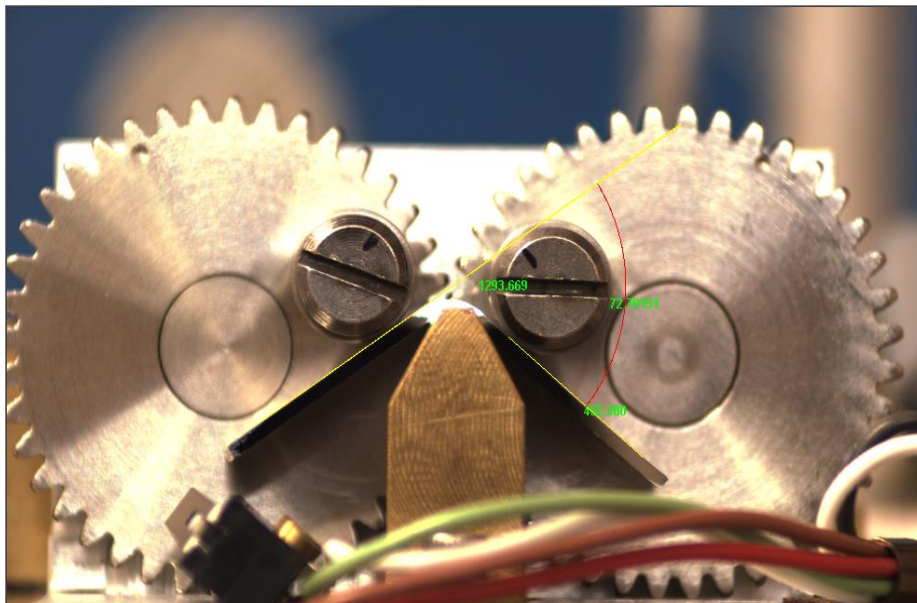

Figure 2. Bending rig

RESULTS

Bending Mechanics

        The neutral axis motion with bending was measured over five columns of the grid centred on the apex of the bend i.e. over 1 mm in the major strain direction. The variation in strain with distance from the upper bend surface, together with upper and lower bounds for individual pairs of spots, for two bend angles, 65 and 142° is shown in Figure 3. The neutral axis, which is at zero strain, moves deeper in to the sample as the bending angle increases. After a bend of 140° it has moved from the middle of the sample about 275 μm further in to the sample.
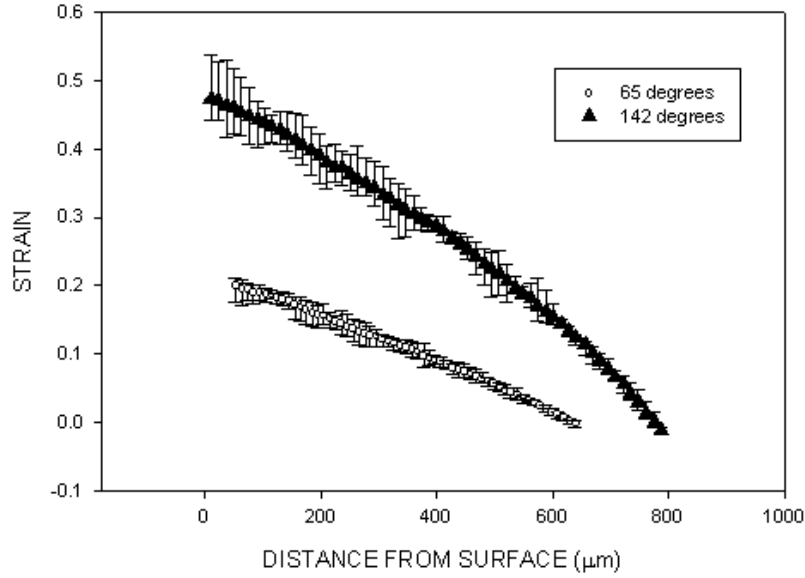
Figure 3. Motion of neutral axis

From bending theory for a purely plastic sheet the neutral axis bend radius, r_n , is given by:

$$r_n = t(k^2 + k)^{1/2} \qquad\qquad (1)$$

where $k = r/t$ with r being the measured bend radius and t the thickness of the sheet. In the present case t = 1mm and converting the bend angle to bend radius the predicted neutral axis radius and hence its position in the sheet can be obtained. Figure 4 compares theory with experiment and it can be seen that theory underestimates the extent of neutral axis motion.
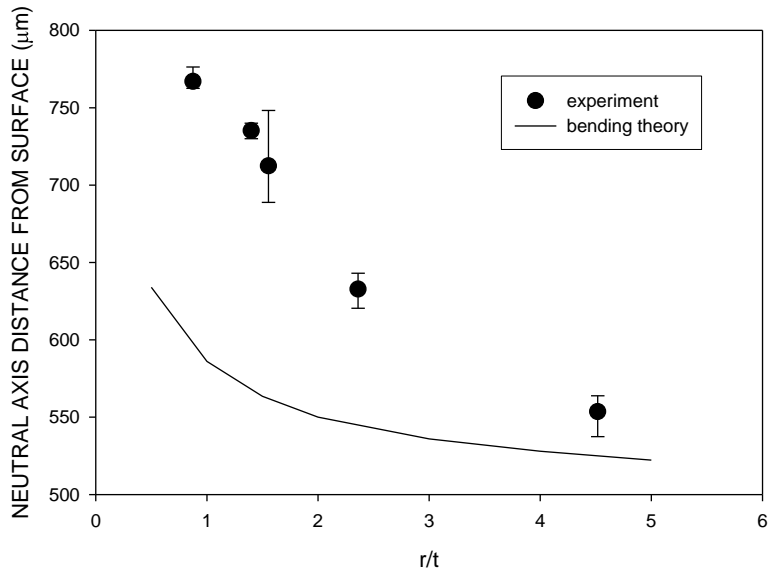
Figure 4. Neutral axis motion, experiment and theory

Maximum Strain

The maximum strain in the through thickness direction occurs at the outer bend surface and to get a measure of this the strain has been measured 10 μm below the surface. For plane strain deformation and a moving neutral axis the maximum strain, ε_S is given by:

$$\varepsilon_S = \ln[(r + t)/(r + g)] \tag{2}$$

where $(r + g) = [r(r + t)]^{1/2}$. Figure 5 compares theory with the experimental results and while the theory underestimates the maximum strains, they are in quite good agreement.
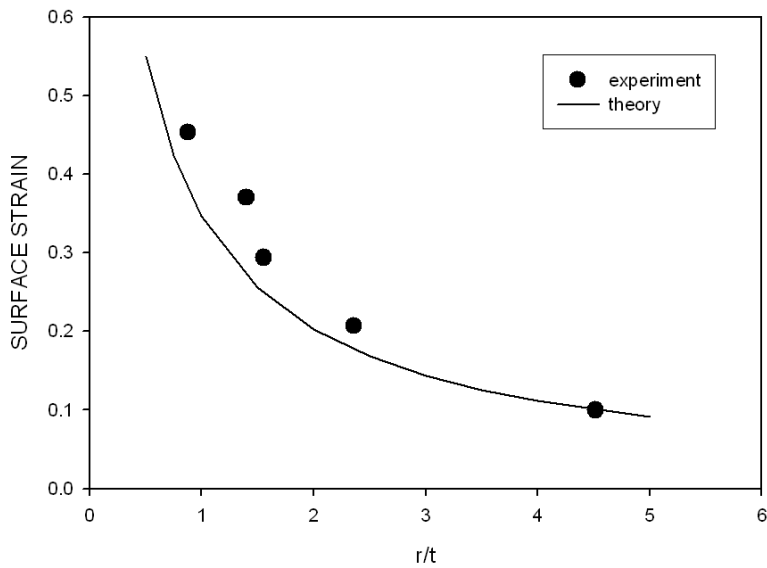

Figure 5. Maximum surface strain with bend angle

Plasticity on the Bend Surface

       The appearance of the grid on the upper bend surface after a 36° bend is shown in Figure 6. While overall the grid reflects plane strain deformation, the grid exhibits distortion on a local scale reflective of the expected inhomogeneous deformation. Slip lines are apparent within grains and displacement out of the surface is apparent at some grain boundaries.
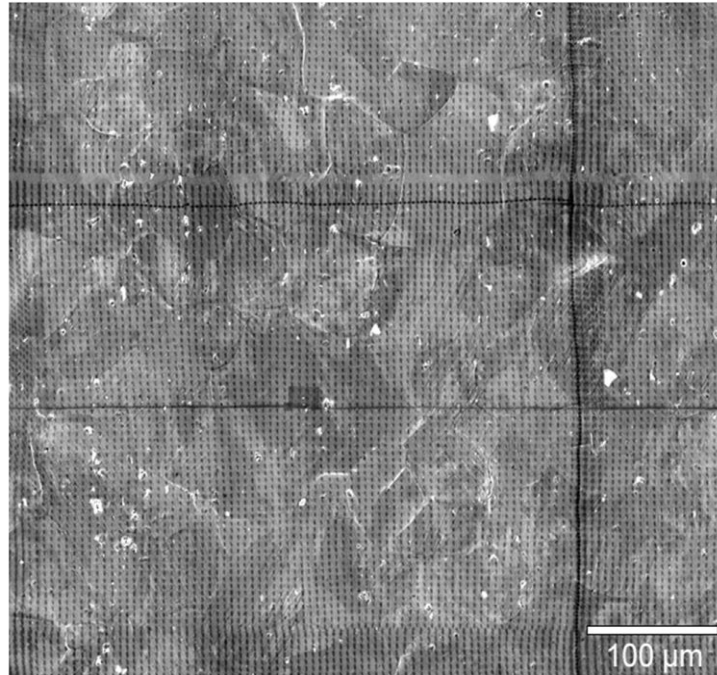

Figure 6. Grid after 36° bend

       As bending progresses slip bands intensify within grains, more grain boundaries exhibit surface displacement and eventually micro-cracking occurs at intermetallic particles, intense slip bands and some grain boundaries (Figure 7). Even at bend angles as low as 15° displacement occurs at some grain and the FIB image in Figure 8 shows the displacement in more detail.
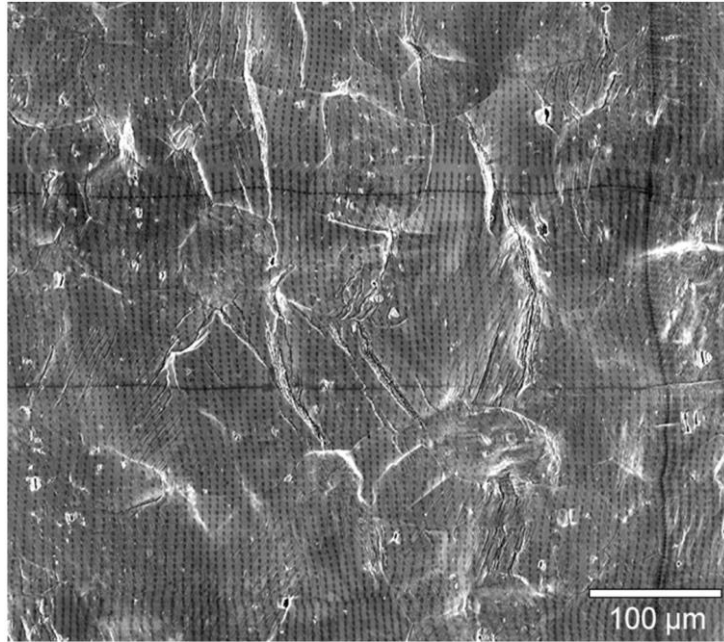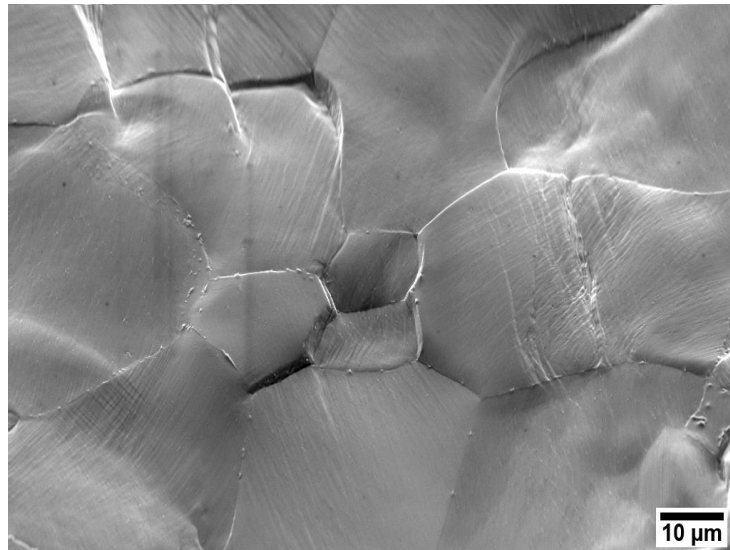
Figure 7. Surface damage at 99° bend

Figure 8. Displacement at grain boundaries

The plasticity associated with the grain boundary displacement has been considered in a previous publication (Lloyd et al., 2010), where the local strain associated with the displacement was shown. Analysis of the misorientation across several hundred grain boundaries exhibiting displacement did not indicate that there are any particular misorientations associated with phenomenon.

The evolution of local strain development on the bend surface with bending across the apex of the bend is shown in Figure 9, where it is apparent that strain localization occurs from a bending of about 30°, intensifying as bending progresses and exceeding values of 0.5, keeping in mind that this sample has not yet developed a macroscopic fracture.
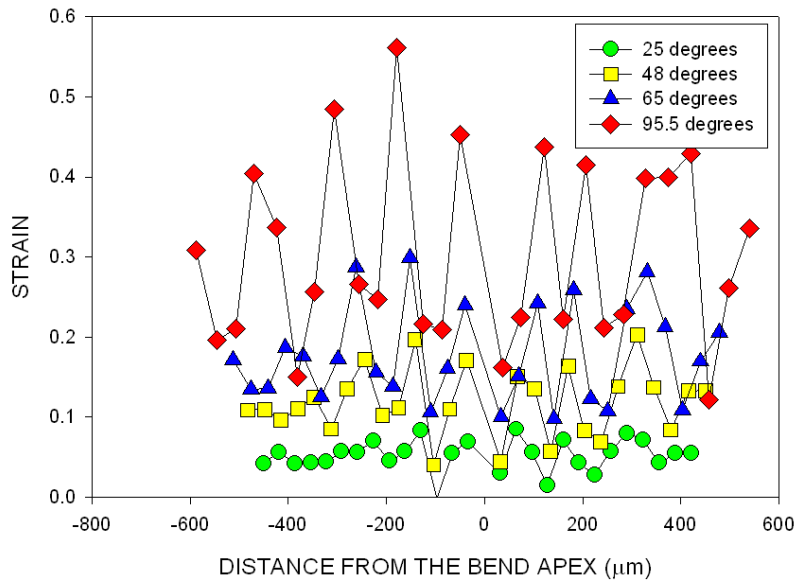
Figure 9. Strain distribution for various bend angles

Predicting Bendability

The previous results demonstrate that bendability is controlled by fracture on the upper bend surface, even though "damage" in the form of voiding and particle cracking may occur prior to this. This is precisely what Datsko and Yang suggested (Datsko and Yang, 1960). They proposed that fracture under bending occurs when the surface strain of the bend exceeds the fracture strain of the alloy and developed the expression:

$$r/t = (C/RA) - 1 \tag{3}$$

where RA is the fracture strain for the alloy and C is a constant in the range 60– 0% when RA is in percent. Since sheet bending is plane strain deformation the fracture strain should really be measured under plane strain but since the difference in fracture strain between tensile and plane strain is generally small in Al alloys, using the tensile fracture strain will only require a small adjustment in C.

Many studies in Al alloys are in agreement with equation (3) for T4 or O temper alloys and Figure 10 shows that this is also the case for aged AA6111.
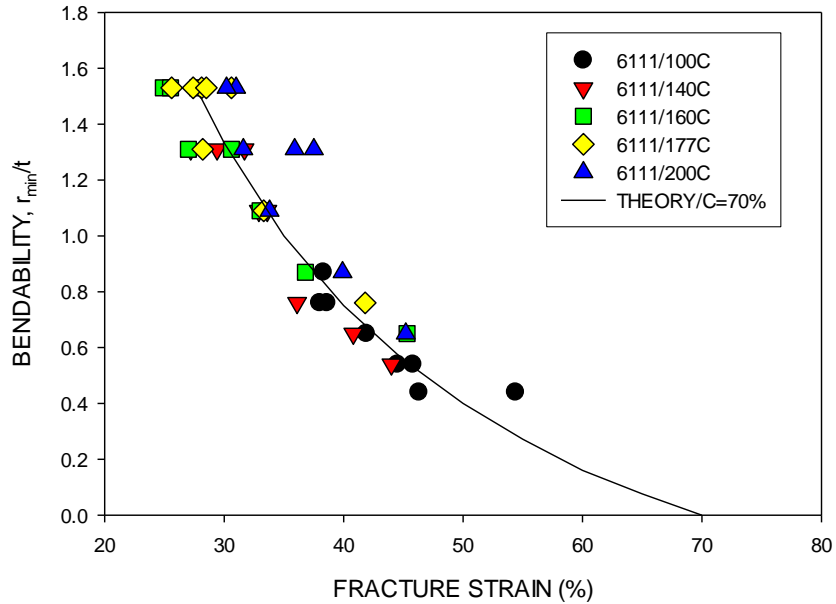
Figure 10. The relationship between bendability and fracture strain

DISCUSSION

The neutral axis experiments show that in this alloy, which exhibits extensive plasticity during bending, the neutral axis moves further in to the specimen as bending progresses. The theoretical expression for the movement underestimates its extent. This means that any damage associated with bending, such as voiding and particle cracking, may extend further in to the sample than expected. The level of maximum strain at the upper bend surface is also underestimated by the theory but in this case the difference is quite small and using the theoretical expression gives a reasonable estimate of the level of strain. The theoretical expressions were developed assuming essentially elastic – plastic deformation, ignoring issues of work hardening or strain inhomogeneity, so the discrepancy between theory and experiment is not unexpected.

The microstructural development of plasticity shows the usual features of slip bands initially, with subsequent development of shear bands within the grains as bending continues. An additional deformation feature from low bend angles is significant surface displacement at grain boundaries. This feature has been noted in micrographs in previous bending studies and also in tensile deformation at large strains (Subedi et al., 2015). The outer bend surface is subjected to large strains and the grains on the surface are unconstrained, enabling the displacement to occur. Previous work (Lloyd et al., 2010) indicated that the displacement is accomplished by extensive local shears and this is reflected in the distortion of the contamination grid in the region of the displaced boundaries. The number of boundaries exhibiting displacement increases with bend angle, while the misorientation across the displaced boundaries cover the whole range of expected grain misorientations. This is a plasticity mode that needs further study and the strains involved at the boundaries can be very high and eventually some of the boundaries fail. Bendability in these heat treatable alloys is very sensitive to quench rate, as shown in previous studies and this is not surprising with the extensive strains developed at the boundaries. At the highest bend angles cracking of intermetallic particles and within shear bands and grain boundaries, leads to final macroscopic crack development. None of these plasticity features are particularly unique to bending, occurring in most failure modes, but the issue of an unconstrained surface, which allows for grain to grain displacement, together with extensive shear band formation as a result of the plane strain deformation and strain gradients and finally the high strains that can be achieved in the absence of geometrical instability or necking, make some of the features more apparent.

The bendability is consistent with the Datsko and Yang analysis which assumes that bend failure occurs when the outer surface of the bend exceeds the fracture strain of the sheet. This enables the potential of a sheet to achieve any particular bend required to form the part to be assessed. Knowing the bend radius associated with the part, equation (2) can be used to calculate the strain and if this strain value is exceeded by the fracture strain the part can be formed without bend failure. Different alloys can also be compared using plots according to equation (3). Previous work has also shown that, provided the microstructure relevant to the fracture process remains constant, the fracture strain scales with the yield stress (Lloyd, 2003). An example of this relationship for aged AA6111 is shown in Figure 11.
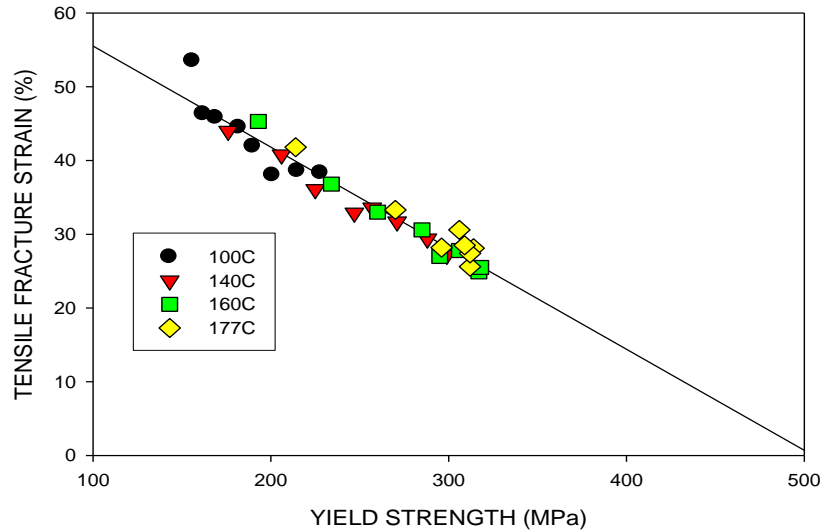

Figure 11. Variation of fracture strain with yield strength for different levels of aging

So if the relationship between fracture strain and yield stress is known, the variation of bendability with yield stress can also be established. The yield stress – fracture strain is given by:

$$RA = B + m\sigma_Y \tag{4}$$

where σ_Y is the yield stress, RA is the fracture strain and B and m are constants. Substituting equation (4) in to equation (3) gives for bendability, r/t,

$$r/t = [(C/(B + m\sigma_Y)] -1 \tag{5}$$

So one can interpolate between the different relationships to assess the bendability.

Finally, there is a caveat to what has been discussed. As noted earlier, the neutral axis moves when extensive plasticity occurs during bending and the maximum strain can be obtained from equation (2). However, if plasticity in the alloy is limited the neutral axis is static and remains at the mid-thickness position. In this case the maximum strain for a static neutral axis, ε_{SN}, is given by:

$$\varepsilon_{SN} = \ln[(r + t)/(r + t/2)] \tag{6}$$

and this has to be used to calculate the outer surface strain. For high strength tempers in 2000 and 7000 alloys the plasticity will be very limited but the fracture strain still determines bendability.

SUMMARY

The experiments demonstrated that the equation to describe the motion of the neutral axis under-estimates the extent of the axis motion, as does the expression for the maximum strain at the outer bend surface but in this latter case the under-estimate is relatively small and the equation can be used to give a reasonable estimate of the strain involved. At the micro-level the strain is very inhomogeneous with large strain gradients developed at shear bands and grain boundaries, with strain localization beginning at even low bend angles. At the surface extensive displacement occurs at the grain boundaries since the deformation is unconstrained. At the highest bend angles or bend radii, strain levels can approach 0.7, intermetallic particles crack and voids form, while failure also occurs within shear bands and grain boundaries. All of these fracture modes occur at high strains in other deformation processes.

The bendability is limited by the fracture strain of the alloy being exceeded at the outer bend surface. If the fracture strain of the alloy is known, the bendability of any particular alloy sheet can be established.

REFERENCES

Becker, R. (1992). An analysis of shear localization during bending of a polycrystalline sheet. *J. Appl. Mechan., 59*, 491–496.

Datsko, J. & Yang, C.T., (1960). Correlation of bendability of materials with their tensile properties. *J. Eng. Indus., 82*, 309–314.

Geist, G.J. & Parker, B.A. (1984). Experimental studies of the strain distribution in bends from Al sheet. *J. Mech. Working Techn., 9*, 201–207.

Hoffman, O. & Sachs, G. (1953). Theory of Plasticity, McGraw Hill, p.268.

Lloyd, D.J. (2000). Ductility and bending in 6000 series alloys. In S.K. Das (Ed), Automotive Alloys 1999, The Minerals and Metal Society (pp. 211–221).

Lloyd, D.J. (2003). The scaling of the tensile ductile fracture strain with the yield strength in Al alloys. *Scripta Mater., 43*, 341–344.

Lloyd, D.J., Evans, D., Pelow, C., Nolan, P., & Jain, J. (2002). Bending in All alloys AA6111 and AA5083 using the cantilever bend test. *Mater. Sci. & Techn., 18*, 621–628.

Lloyd, D.J., Steele, D., & Huang, J.H. (2010). Plasticity associated with grain boundaries during the bending of an Al-Mg-Si based alloy. *Scripta Mater., 63*, 426–429.

Lubhan, J.D. & Sachs, G. (1950). Bending in an ideal plastic material. *Trans ASME*, 201–208

Mattei, L, Daniel, D, Guiglionda, G., Klocker, H. & Driver, J. (2013). Strain localization and damage mechanisms during bending of AA6016 sheet. *Mater. Sci. & Eng. A, 559*, 812–821.

Shi, Y., Jin, H., Wu, P.D., Lloyd, D.J. & Embury, J.D. (2014). Failure analysis of fusion clad alloy system AA3003/ AA6XXX sheet under bending. *Mater. Sci. & Eng. A, 610*, 263–272.

Subedi, S., Pokharel, R. & Rollet, A.D. (2015). Orientation gradients in relation to grain boundaries at varyig strain level and spatial resolution. *Mater. Sci. & Eng. A, 618*, 348–356.